Capitalizing on Heterogeneity and Anisotropy to Design Desirable Hardware That is Difficult to Reverse Engineer

Stephen P. Harston
e-mail: sharston@gmail.com

Christopher A. Mattson[1]
Assistant Professor
e-mail: mattson@byu.edu

Brent L. Adams
Professor
e-mail: b_l_adams@byu.edu

Department of Mechanical Engineering,
Brigham Young University,
Provo, UT 84602

This paper presents a method for treating material microstructure (crystallographic grain size, orientation, and distribution) as design variables that can be manipulated—for common or exotic materials—to identify the unusual material properties and to design devices that are difficult to reverse engineer. A practical approach, carefully tied to proven manufacturing strategies, is used to tailor the material microstructures by strategically orienting and laminating thin anisotropic metallic sheets. The approach, coupled with numerical optimization, manipulates the material microstructures to obtain the desired material properties at designer-specified locations (heterogeneously) or across the entire part (homogeneously). A comparative study is provided, which examines various microstructures for a simple fixed geometry. These cases show how the proposed approach can provide hardware with enhanced mechanical performance in a way that is disguised within the microscopic features of the material microstructure.
[DOI: 10.1115/1.4001874]

1 Introduction

The optimization of macroscopic geometry, known in the literature as size [1], shape [2,3], and topology [3,4] optimization, is a powerful approach to identify hardware with desirable performance characteristics [5]. A different, yet equally powerful, approach is to manipulate microscopic metallurgical material characteristics to enhance the material properties and achieve desirable hardware performance [6]. Individually, these two approaches have improved products and allowed for more advanced designs over those of the past [5,6]. Through an integrated approach, however, macroscopic *and* microscopic features can be manipulated in a complementary way to develop hardware designs with a mechanical performance that can only be obtained with an integrated approach. These designs can exhibit desirable behavior that is not intuitively understood, or easily replicated and are of particular interest to those who wish to make their designs more resistant to reverse engineering [7].

While others have previously coupled material properties of metals with geometry and performance optimization [8–12], we present a new method of tailoring the properties of metals by using thin metal laminations strategically oriented [13] and ultrasonically welded together [14]. We show how numerical optimization can be used to search through a material design space [15–17], and that the proposed integration of optimization, manufacturing, and design methods can result in material microstructures that are consistently producible from a manufacturing perspective. The proposed method can, therefore, be used to tailor new and practical materials for the design engineer's specific need.

For many product designers, material properties, such as the yield strength and Young's modulus, are chosen from a set of discrete values, typically published in the form of a table of material properties [18]. Under this typical approach, if one requires a part to withstand more stress before failure, the geometry is typically changed or a new material class or alloy is selected. Consider the benefit that would come to the design engineer if he or she could hold the geometry constant and, using the original material, improve the material's resistance to plastic failure or other material properties. He or she could increase the product performance without resorting to more expensive materials or they could hide performance increases from competitors, since discovering the source of the increased performance would not be trivial. This paper proposes a methodology to do this.

Recent advancements in material science enable the development of the proposed approach [13,19]. Specifically, these advancements pertain to the material microstructure, which is the composition of a material including arrangement, size, orientation, and distribution density of crystallographic grains [19]. These advancements have led to predictive relationships for characterizing the material properties as a function of the material microstructure. When coupled with numerical optimization and lamination technology (two other key enablers), the material properties can be modified as simple as its geometry, creating one more degree of freedom in the design. Additionally, the method outlined in this paper allows one to make calculated changes in the microstructure to obtain the desired results in the material properties at designer specified locations (heterogeneously) or across the entire part (homogeneously).

It is known that one or more microstructures can be used as a starting point to obtain any combination of properties in the *property closure*, which is the set of all theoretically possible material properties [19]. Unfortunately, it is not known how to consistently manufacture all microstructures required to obtain every combination of properties in the property closure. Therefore only a small, discrete set of material properties contained within the full property closure are commonly used in practice. This is one of the main reasons why material properties are rarely considered continuous variables in the material selection activities of product design. With the use of laminations, microstructures that were previously difficult to obtain become simple combinations of optimally layered, well-known microstructures [13], as presented in this paper.

The proposed process is similar to carbon-fiber composite material designs, where many thin layers are ideally aligned to obtain

[1]Corresponding author.
Contributed by the Design for Manufacturing Committee of ASME for publication in the JOURNAL OF MECHANICAL DESIGN. Manuscript received March 26, 2009; final manuscript received May 24, 2010; published online July 12, 2010. Assoc. Editor: Michael Kokkolaras.

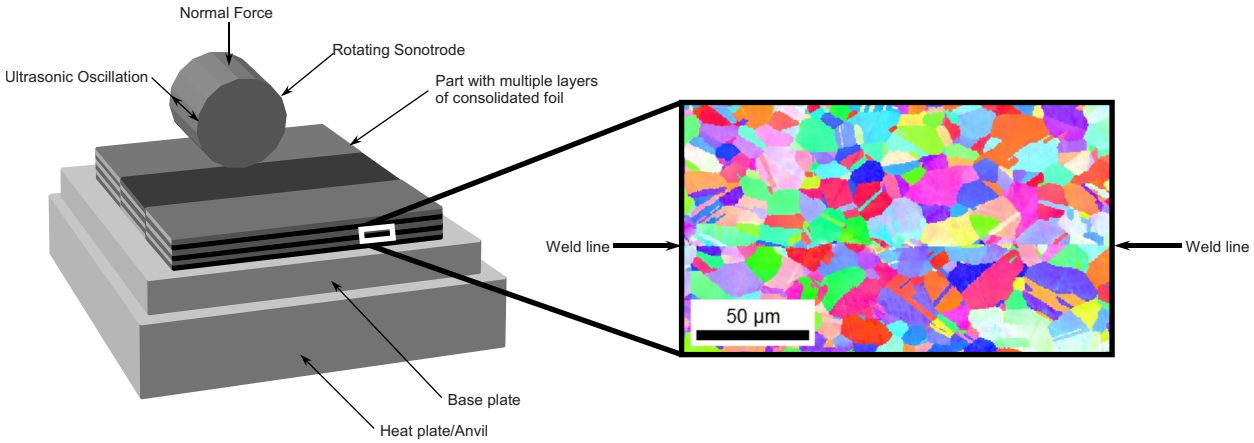

Fig. 1 Ultrasonic consolidation process with scanning electron microscope image of grains at the layer interface

the desired material properties in specific directions [20,21]. Studies in carbon-fiber composite materials design have considered the effects of material microstructures on product performance for years [20]. Specifically, fiber composites have been analyzed and tested to determine fiber composition, epoxy composition, fiber/epoxy mixtures, and layer orientation resulting in the desired product performance [20–23]. Some have even studied the effects of alternating layers of fiber/epoxy and thin metal sheets [24].

Significant contributions have also been made by others who have recognized performance improvements that can be achieved by microstructure design with metals [8–10,25,26]. While the origins of the modern theories used for analyzing metallic microstructures may be traced back to the mid 1900s, it is only in recent years that microstructure theories have matured to the point that enables the design of metals at the microlevel, resulting in a desired macrolevel performance [25]. Notably, McDowell [25,26] discusses the challenges when designing the microstructure plasticity characteristics and also presents a methodology that effectively overcomes microstructure design challenges [8]. Olson [9], and Kuehmann and Olson [10] discussed the computational design of materials to meet specific engineering needs. Specifically they address the handling of conflicting design objectives and expensive computations to obtain the desired material properties and desired product performance.

The purpose of this paper is to present a new design framework, in conjunction with numerical optimization, which couples microstructure manipulation and modeling with existing manufacturing processes to create products with desired performance. The microstructure sensitive design approach, as presented in this paper, enables a product to perform (e.g., deflection, yield characteristics, shear characteristics) in a way that cannot be obtained without manipulating the material. Furthermore, the source of performance improvement is difficult to determine and recreate from a reverse engineering perspective, thus impeding competitors from successful reverse engineering.

The design framework presented in this paper is based on the published work of two fundamental elements: microstructure characterization [13,19,27] and the additive manufacturing process of ultrasonic consolidation (UC) [14,28,29]. While microstructure characterization and ultrasonic consolidation have been previously described in the literature, in this paper they are coupled under an optimization framework that enables the creation of products with enhanced mechanical performance.

The framework proposed in this paper is presented by first reviewing enabling technologies and fundamental theories supporting the work. This is presented in Sec. 2. Section 3 then describes the design framework used to obtain desired material properties with common materials. In Sec. 4, a comparative study is provided, which examines various microstructure implementations for a simple fixed geometry. Concluding remarks are provided in Sec. 5.

2 Description of Enabling Technologies and Fundamental Theories

In this section we present the enabling technology of ultrasonic consolidation [14], which facilitates the joining of thin metal sheets with minimal disturbances to the microstructure in the weld areas. We also present four fundamental theories required for predicting the material properties for a part, based on the measurements of a material's microstructure. They are as follows: reference frames, fundamental zone, rotations of anisotropic layers, and the lamination of those thin layers.

2.1 Ultrasonic Consolidation: Additive Manufacturing Process of Metals. One manufacturing technology that allows improved material properties to be obtained from common metals is the additive manufacturing process of UC. UC utilizes the principles of ultrasonic welding [14] to combine metal sheets, typically 150 μm thick, in a layer-by-layer process. This process is often combined with a three-axis computer controlled mill to produce complicated geometry during the additive process. The UC process, as represented in Fig. 1, begins with a heated base of the same material of the part. A rolling/rotating sonotrode applies a normal force while oscillating, which results in dynamic interfacial stresses at the interface between the two mating surfaces [14,28,29]. The stress incurred by the high frequency oscillations, around 20 kHz, produces elastic-plastic deformation and establishes a metallurgical bond, as can be seen in the polished cross section shown in the right side of Fig. 1. This process is repeated layer-by-layer until the part is completed with the desired number of layers.

It is impressive to note that UC materials can yield a 85–100% linear weld density along the bonded interface [30]. A linear weld density of 100% implies that the weld has an equivalent void space, dislocations, and is as durable (both for fatigue and corrosion resistance) as the surrounding grain boundaries. Obtaining a linear weld density of 100% is feasible; however, it requires proper adjustment of the UC manufacturing parameters (e.g., magnitude of the oscillations, frequency of sonotrode, normal force applied), which are typically determined through empirical studies on the material of interest [31,32]. When the linear weld density is not 100%, products may need to be designed with a larger safety factor to take into account the weakened welds, which may result in decreased fatigue life and yield strength.

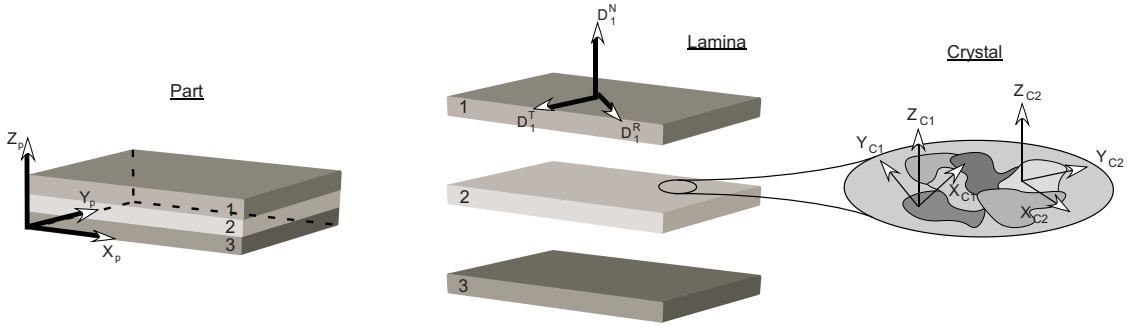

Fig. 2 Reference frames defined for the part, lamina, and crystal

However, Ram et al. [31,32] conducted numerous experiments with ultrasonically consolidated materials to determine the optimal parameters to obtain a linear weld density of approximately 100%.

One important characteristic of UC is the low temperature at which the layers are welded together, which range from ambient to 350°F. This results in minimal local disturbances in the weld area, thus making the layer-by-layer construction virtually undetectable, which supports the notion of hiding the source of performance increases from competitors.

Possibly the most impressive feature of UC is the number of microstructures that may be obtained thereby. It is known that extreme microstructures may be induced in metal foils by rolling and recrystallization [33]. These foils may then be combined by the UC process to create a material made with laminations. When layers with known microstructures are strategically placed, one can effectively create a laminated material with desired properties and even consistently obtain material properties that are otherwise not used in practice.

As the additive process of ultrasonic consolidation is relatively expensive compared with traditional manufacturing processes (e.g., rolling, heat treating, machining), it is often best strategically implemented into a few critical components of a system. The quantity of components that are created with the UC process will adversely affect the product manufacturing cost; however, (i) UC enables designers to obtain microstructures (and therefore, the desired material properties) that are difficult, if not impossible, to obtain by other means, and (ii) when critical components of a system are made difficult to reverse engineer, by using UC to obtain unusual microstructures, it effectively impedes the reverse engineering of the entire system. Therefore the costly nature of UC can be justified in some cases by the unique benefits it brings.

2.2 Reference Frames and Fundamental Zone Defined. As the UC method forms a basis for microstructure manipulation by joining laminae, it is useful to define three reference frames commonly used when working with laminae: crystal, laminate, and part reference frames. The main purpose of these reference frames is to have a consistent point of reference when aligning the layers and defining directionally dependent material properties. While it is important that reference frames do not vary over the design process, it does not matter how reference frames are oriented. There are, however, common approaches for orientation; typically the crystal's reference frame will be aligned with the crystallographic directions X_{cj}, Y_{cj}, and Z_{cj} for the jth crystal in a sample [34], where the subscript c represents the crystal frame.

A convenient reference direction for a heavily rolled lamina is the rolling direction. One axis of the sample reference frame is aligned with the rolling direction and is termed as the "rolling direction" or D_k^R for the kth layer. The second axis, or the "normal direction" (D_k^N), is placed perpendicular to the both the rolling direction and a surface of the laminate. While it does not matter which surface is selected for the thin lamina, typically surfaces with a large surface area are used as a reference. With two axis defined, the third axis, the "transverse direction" (D_k^T), is defined with the use of the right-hand rule [19].

The final reference frame to be described, which is the part reference frame, is defined according to the geometry and is typically aligned with a dominant geometric feature, as seen in Fig. 2 as X_p, Y_p, and Z_p. The part reference frame allows one to properly align the rotated laminae in relation to the part to achieve the desired properties in the directions of interest [34].

The orientation of one reference frame to another is represented by the standard Euler angles ϕ_1, Φ, and ϕ_2. The Euler angles represent all possible orientations but due to symmetry, the limits on the angles may be set to $0 \leq \phi_1 < 2\pi$, $0 \leq \Phi \leq \pi$, and $0 \leq \phi_2 < 2\pi$, respectively [34]. For parts constructed with layers, it is convenient to only rotate the layers about their normal axes, which is what we do in this paper.

Another important concept in being able to extract material properties from crystal orientation data is the fundamental zone (FZ). The FZ is the set of all physically distinct orientations of the local crystal that can occur [19]. Due to the computational power required to analyze the infinite number of possible crystal orientations, the FZ is binned into groups of orientations with each bin approximated by a single orientation. The binned fundamental zone (BFZ) can then be used as a simplified orientation description for all crystals in the sample. The number of bins is determined by the conflicting objectives of the desired accuracy and computational time available.

2.3 Using the Rotation and Lamination Theory to Predict the Material Properties. In this section we present the microstructure-to-material-properties theory, which is the process we used to predict the material properties, given the information about the material microstructure. In the rotation and lamination theory presented below in Sec. 2.5, it is through manipulation of the material microstructure of each layer that one is able to obtain an overall change in the material properties and product performance. Therefore, it is important to understand the microstructure-to-material-properties theory, which is the crucial link in considering the material properties as design variables.

The flowchart in Fig. 3 presents the process in which material stiffness $\bar{C}_{wxyz}$ is determined from the microstructure properties of a material. As a note, other specific material properties such as the yield strength, Young's modulus, Poisson's ratio, shear modulus, and critical resolve shear stress can also be determined from the material microstructure by a similar process if desired. The flowchart in Fig. 3 is now described in detail.

The process to determine the material stiffness begins by initializing the variables shown in the upper left box of Fig. 3 and by obtaining the material specific constants from the literature such as C_{11}, C_{12}, and C_{44} [35]. Next, the FZ is binned, allowing multiple orientations to be approximated by a single orientation, thus decreasing the number of unique orientations requiring analysis.

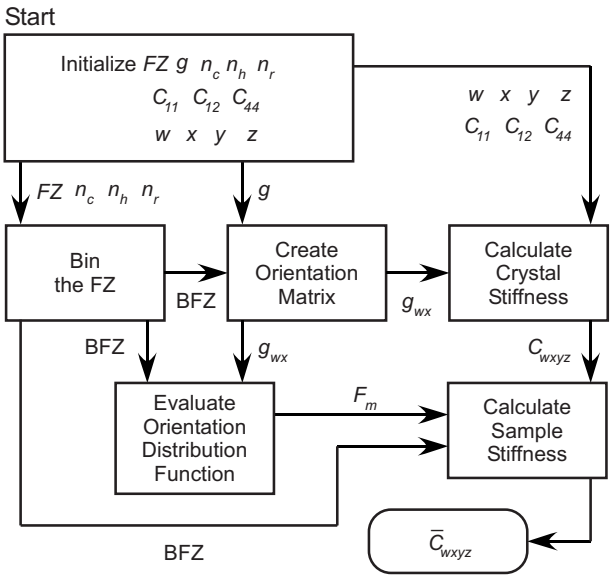

Fig. 3 Microstructure-to-material-properties flowchart

The resolution of the binning is determined by dividing the FZ into a number of rows, columns, and layers represented by n_r, n_c, and n_h, respectively. Fewer bins equate to a faster computational time with a decrease in accuracy while increasing the number of bins improves accuracy at the expense of time. Continuing downward from the box depicting the binning of the fundamental zone, the Fourier coefficient F_m is calculated, which is literally the volume fraction of crystals in the mth bin of the BFZ. Simply stated, F_m is the percentage of crystals that are aligned in a given direction and is used for calculating the material stiffness. Before F_m can be calculated, crystal orientation data g obtained by orientation image microscopy (OIM) [19] is converted to an orientation matrix g_{wx}, which forms a link between the raw OIM data and the BFZ. One of the key factors in obtaining a continuous range of material properties is the understanding of the initial microstructure as determined by OIM. Without the details of the starting microstructure (characterized by g in the upper left box of Fig. 3) for the specific material to be used, the desired material properties cannot be obtained with the rotation/lamination theory.

A simple way to determine the percentage of crystals occupying a bin is to use the orientation distribution function (ODF). The ODF is a function that receives information about the BFZ and orientation matrix g_{wx} and enables a description of all crystal orientations in a sample. Evaluating the ODF with a single direction results in a scalar representing the percentage of crystals aligned in that direction. When the ODF is calculated for multiple directions, the results are a scaler representing the percentage of crystals aligned in the multiple directions defined—such is the case of a bin in the BFZ.

As is true with all material properties, stiffness of the sample is a function of the stiffness of each crystal. In fact, the sample stiffness $\bar{C}_{wxyz}$ is simply the average stiffness of all crystals. Parameters required to determine the crystal stiffness are the direction of interest as defined by the designers (w,x,y,z) and three material properties, which come from the literature C_{11}, C_{12}, and C_{44}. Note that the additional parameters related to binning the fundamental zone are not required unless reducing the computation cost is required. With F_m and C_{wxyz} known, it is a simple matter to compute for $\bar{C}_{wxyz}$, since $\bar{C}_{wxyz}$ is the average stiffness weighted by F_m.

2.4 A Criteria for Plastic Failure. The failure criteria used in this paper to determine if the material plastically deforms under the applied loading conditions is presented in this section. Two approaches can be taken to characterize plastic failure; the first involves developing a general estimate of the material's yield strength, which can be found directly from microstructure data and calibrated with a single tensile test. Another approach uses the classic power law viscoplasticity failure model, which requires both material microstructure information and loading conditions. In this paper, we use the viscoplasticity failure model, which can be expressed as

$$\bar{D}_{ij} = D_{ij} = \dot{\gamma}_0 \sum_{s=1}^{S} \left| \frac{(\sigma'_{kl})\alpha_{kl}^{(s)}}{\tau^{*(s)}} \right|^n \text{sign}((\sigma'_{kl})\alpha_{kl}^{(s)})\alpha_{ij}^{(s)} \tag{1}$$

where $\dot{\gamma}_0$ is the reference shear rate, S is the total number of slip systems in the material, σ'_{kl} is the local deviatoric stress for a given direction [36], $\alpha_{kl}^{(s)}$ and $\alpha_{ij}^{(s)}$ are simple combinations of the slip directions and the slip plane normals [36], and $\tau^{*(s)}$ is the critical resolved shear stress as calculated from the Hall/Petch relationship [37]. The only value on the right side of the equation that cannot be obtained from literature is the local deviatoric stress, which can be determined using finite element analysis with known loading conditions. The local strain rate D_{ij} can then be calculated. One assumption often made when using the viscoplasticity failure model is that the average of the local strain rates is equivalent to the macroscopic strain rate $\bar{D}_{ij}$ of the material at that point. Therefore plastic deformation of a material is directly related to the material strain rate. It follows that when

$$D^* \leq \bar{D}_{ij} \tag{2}$$

where D^* is the critical strain rate, we can know that the material has plastically deformed at that point. In the current paper, we have selected the critical strain rate to be $0.001s^{-1}$. The finite element analysis returns the stress at each node, which we use to determine the total number of nodes that was yielded by the relationships above. As there will always be some quantity of nodes that fail under any loading condition, we specify that a material fails when 15% or more of the nodes have plastically deformed. For the full development and application of Eq. (1), the reader is referred to Refs. [27,36,38,39].

2.5 Part Construction by the Rotation and Lamination Theory. We now consider approaches by which microstructures can be intentionally created to have certain characteristics. We have explored a variety of manufacturing processes that allow for microstructure manipulation such as friction-stir welding [40], heat treatment, and introducing voids into the material. While these processes may be utilized in many different ways, strategically orienting and laminating thin sheets is a more flexible and predictable way to consistently obtain designer selected values of the material microstructures. The theory of rotations and laminations allows one to take any initial microstructure and create a new microstructure by stacking and welding thin metal layers—with directionally dependent material properties—at specific rotations. This theory, coupled with UC technology, allows the designer to hold the alloy fixed, yet modifies the material properties by choosing the layer configuration and orientation.

Recall that the material property closure is the set of all material properties that are possible if one could create all possible microstructures. Since not all microstructures are practically obtainable, the achievable space in the property closure is limited. Implementation of rotation and lamination theory, however, greatly expands the achievable space in the property closure, as shown in Fig. 4 for Ni 201. The axes shown in Fig. 4 represent two different material properties: material compliance (elasticity) on the x-axis and yield strength on the y-axis. Note the subscripts that represent the desired directions for which the properties apply. The outermost loop, and the area it contains, represents every possible combination of these two properties. A single point represents a specific value for both the compliance and the yield

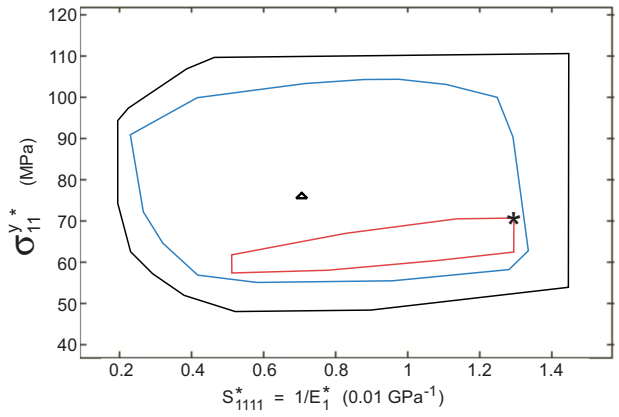

Fig. 4 Property closure of yield strength versus compliance for Ni 201. The outer loop is the property closure, the triangle represents an isotropic material with the same material properties in all directions, and the inner loop represents all material properties that can be obtained by applying the rotation and lamination theory to a material that starts with the microstructure shown as a star. The middle loop represents the material properties that can be obtained when the layer rotations are not constrained to a single plane.

strength, which may be mapped to one or more microstructures that will have those properties. The triangle in Fig. 4 represents isotropic material properties for Ni 201 while the star represents the starting microstructure of the material—as defined by OIM—in the direction of interest. As a note, the starting microstructure is the material microstructure for a thin metal sheet before reorientation or inclusion in a laminae. The inner loop that intersects the star, and the area it contains for multilayered structures, represents all properties that can be obtained by implementing the rotation and lamination theory to that starting microstructure when all rotations about the normal axis of the respective layer are considered. The remaining loop and the area it contains represents material properties that may be obtained by performing the rotation and lamination process twice (rank 2 lamination) to obtain even more complicated microstructures. It is important to note that any microstructure obtained by conventional methods, such as heavy rolling, can be enhanced to obtain new microstructures and thus enable new combinations of material properties that are typically thought to be unobtainable.

3 Design and Optimization Framework for Enhanced Performance Through Microstructure Manipulation

In this section we present a generic framework that enables us to obtain an enhanced, and desired, mechanical performance created by strategically manipulating the microstructure of common metal alloys using the rotation and lamination theory. Specifically, when given a target performance, the direction(s) of interest, and the desired number of layers, this optimization routine will find an optimal orientation of each layer in an effort to obtain the desired performance in the direction(s) of interest. The generic optimization framework may be seen in Fig. 5(*a*) and a framework specific to structural design, and used in Sec. 4 of this paper, may be seen in Fig. 5(*b*). There are six main parts in the optimization framework, as follows: Part 0: initialization of the system parameters; Part I—gathering microstructure data for the selected alloy; Part II—definition of feasible range of the material properties obtainable by rotations and laminations; Part III—material property exploration and selection using the optimization techniques; Part IV—performance measurement; and Part V—constraint analysis. Each part of the process is now described in detail.

3.1 Part 0: Initialize Input Parameters. Let us first consider Part 0. This part of the framework requires the designer to identify the optimization parameters and variables, and formulate the objective function J. The designer also selects the material class M a specific alloy M_0 from the chosen class to be used as the lamina material, the number of lamina N in the lamination, and at least one direction of interest, which is represented by w, x, y, and z. Assuming a uniform layer thickness, the number of layers required is dependent on the thickness of the part being created.

3.2 Part I: Characterize Microstructure of the Selected Alloy. Before we can obtain the desired material stiffness of a material, we first need to acquire microstructure information about that material. This is done by polishing and scanning the sample with a scanning electron microscope and analyzing the data with OIM software [19]. The data collected includes grain size, grain distribution, grain orientation, and other microstructure information specific to the sample. Once microstructure data are gathered, the range of material properties may be determined, as described in Part II.

3.3 Part II: Determine the Full Range of Material Properties Obtainable with Rotations and Laminations for the Selected Alloy. The range of properties obtainable by rotation and lamination depends on the material microstructure. A material that is isotropic will always have the same properties independent of the material orientation. On the other hand, anisotropic materials made with a single crystal have the most directionally dependent material properties as the properties may change dramatically even with a small rotation. The OIM data found in Part I determines the microstructure of the selected alloy, thus determining the degree of anisotropy that exists in the sample. The OIM data are then used in the rotation/lamination theory to determine material properties in a given direction. Application of the rotation/lamination theory for every orientation from $0-2\pi$ reveals the range of material properties that may be obtained with the sample-specific microstructure. When symmetry exists in the microstructure, the complete range of material properties may be obtained with a reduced set of microstructure orientations. A convex hull encloses the resulting range of material properties and is principally used to help the designer know the feasible range of material properties for the given microstructure. This is the process that was performed on Ni 201 to obtain the property closure in Fig. 4.

3.4 Part III: Determine Rotation/Lamination Strategy Required to Obtain Desired Performance for Selected Alloy. In Part III, we use an optimization routine to determine the manufacturing strategy—specifically the orientation of each layer—to create a laminated material with the desired material properties in the direction of interest. The optimization requires the number of laminations N, the direction of interest, w, x, y, and z, and the objective function, which are all determined by the designer in Part 0. The optimization selects a value of ϕ_1 for each lamina, sends the lamina orientation through the rotation and lamination model, and receives the material properties of interest. The optimizer then sends those material properties to the performance analyzer of Part IV, which evaluates and returns the design objective values μ and/or any other needed analysis such as those pertaining to constraints. Part V evaluates the constraints and determines the magnitude of constraint violation ν. The process is repeated until the optimization determines the optimal orientation of each layer. On the final iteration, the optimization outputs the optimal value of the design objectives μ^*, the constraint violations ν^*, and the optimal orientation of each layer ϕ_1^*. Note that by *optimal* we mean numerically optimal as characterized by the designer-made performance models (e.g., finite element analysis) and characterized by the optimization problem statement, which, in its generic form, is as follows:

$$\min_{\phi_1} J = \{\mu_1, \mu_2, \ldots \mu_{n_\mu}\} \tag{3}$$

subject to

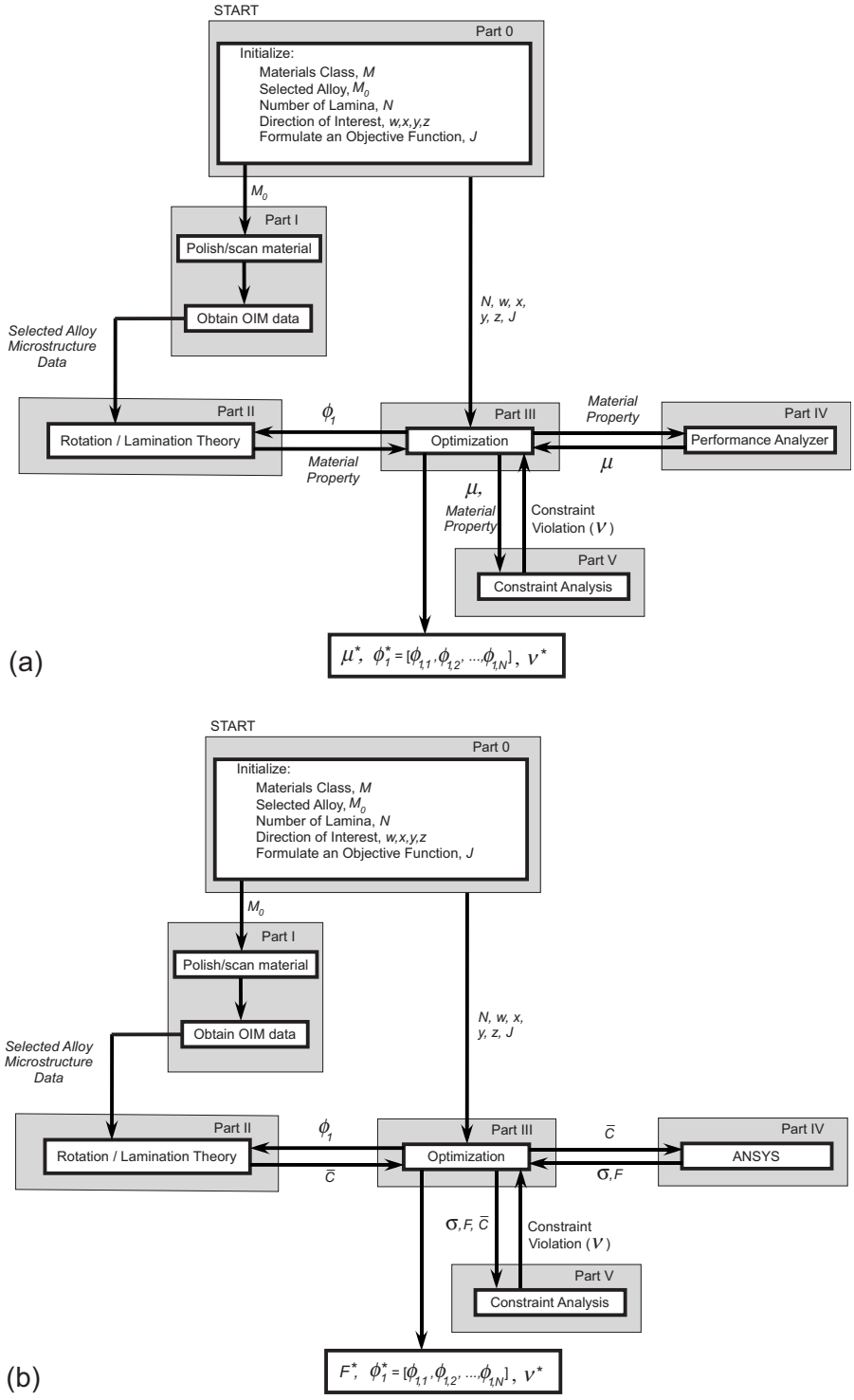

Fig. 5 (*a*) Flowchart of a generic optimization framework to obtain improved performance with common materials; (*b*) an optimization framework specific to the structural stiffness

$$r_q \leq 0, \quad \forall\, q = 1,2,\ldots,n_r \tag{4}$$

$$h_v = 0, \quad \forall\, v = 1,2,\ldots,n_h \tag{5}$$

$$0 \leq \phi_{1,i} \leq \pi, \quad \forall\, i = 1,2,\ldots,N \tag{6}$$

where $\phi_1 = [\phi_{1,1}, \phi_{1,2}, \ldots, \phi_{1,N}]$ and represents the orientation of each layer, and μ_i denotes the ith generic design objective. Note that due to symmetry the design variable is constrained from 0 to π. In some cases, it may be necessary to expand the variable space to avoid active constraints that point to local, as opposed to global, optima.

During the optimization process, each layer is strategically oriented to create a new microstructure in an effort to obtain the desired mechanical performance. If a target material performance is not possible for any combination of the material properties obtainable with the rotation/lamination theory, the optimization rou-

tine will find feasible material properties that result in the best performance possible as measured by the objective function.

3.5 Part IV: Performance Analysis. The performance analyzer in Part IV receives the material properties as determined in Parts II and III, and outputs the design objective values. In the case of structural design (Fig. 5(*b*)), the performance analyzer receives the material stiffness matrix $\bar{C}$ as an input and determines the force required to achieve a prescribed deflection with a predetermined geometry. It also determines the stresses that develop throughout the part as a result of the force. The finite element analysis software ANSYS then returns the force F and the stress σ_i to the optimizer, where i represents the ith node and is used to determine the deviatoric stress σ'_{kl} in Eq. (1).

3.6 Part V: Constraint Analysis. The constraint analysis is a designer-defined function that simply determines if the current design selected by the optimization meets the design criteria. The constraint analysis calculates the constraint violation ν. Returning to the structural design example in Fig. 5(*b*), the constraint analysis will receive the stress (calculated by ANSYS) and the material stiffness, and will determine if plastic deformation has occurred by using the power law viscoplasticity failure model, as described in Sec. 2.4.

Section 3 has illustrated how we use the various theories described in this paper to explore the materials design space and search for the desirable material properties that enhance the mechanical performance. In Sec. 4, we consider a simple mechanical element and show how the use of the aforementioned design and optimization framework leads to desirable mechanical performance—the source of which is hidden in the tailored material microstructure that results from the design and optimization approach.

4 Case Study

This section illustrates the benefits that can come from implementing the theories and methodologies presented in Secs. 2 and 3 of this paper. For this case study, and all substudies presented herein, a simple L-beam geometry, fixed at one end, and exposed to a prescribed deflection at the other, is considered. The L-beam is chosen to illustrate the process because of its simplicity and because it is derived from an actual L-beam designed by one of the authors for a popular mobile phone. As such, the geometry, parameters, and so forth are representative of a realistic industrial application.

We pause now to describe why we fix the geometry throughout this case study and explain the effect this has on reverse engineering. The geometry is fixed for two principle reasons. First, during the design of the L-beam used in the mobile phone, the geometry was already at the upper bounds of a very constrained component envelope. Therefore, any permissible change in the geometry would have an undesirable affect on the performance, as shown below. Second, when a component such as this is reverse engineered by a competitor, the most likely reverse engineering strategy is to copy the geometry and the chemical composition of the material. As shown below, this common reverse engineering approach will not lead to a functional replica. Instead it leads to a design represented by the benchmark design below. A desirable performance can only be achieved through microstructure manipulation. It is important to note that it is unlikely that the competitor will be able to determine the complex material microstructure created by the lamination of independently oriented thin metal foils. Should the competitor determine the complex microstructure, the extremely difficult task of determining how to manufacture that complex microstructure poses yet another barrier to reverse engineering.

Six substudies of the L-beam are provided here for comparative purposes. The illustration provided in Fig. 6 represents the fixed geometry and boundary conditions used throughout the entire case

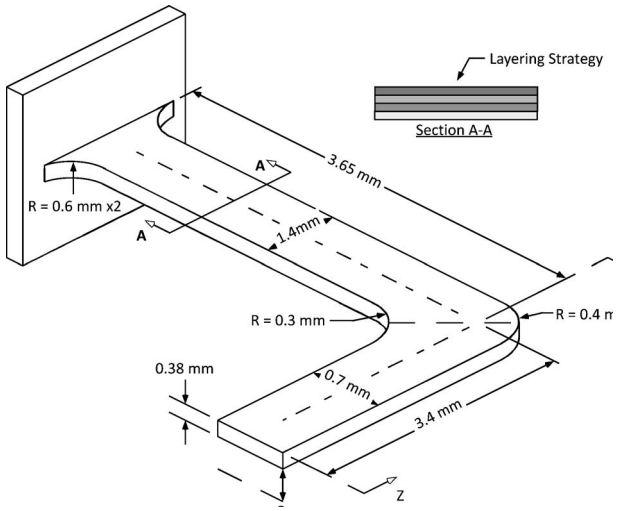

Fig. 6 Geometry and boundary conditions for the L-beam case study

study. The six substudies consider (I) an isotropic one layer lamina, (II) an anisotropic one layer lamina, (III) a multilayered anisotropic laminate, (IV) a heterogeneously distributed microstructure in single layer, and (V and VI) a special exploration into when multilayered laminates out perform single layer lamina and vice-versa. Each substudy shows how the performance of the fixed L-beam geometry can be enhanced by material manipulation.

4.1 Substudies I–IV. For substudies I–IV, the design objective is to minimize the reaction force (in the normal direction) at the free end of the beam, when subject to a prescribed displacement (δ) at the free end and subject to the material being within acceptable yielding conditions. As a note, for applications such as those of the mobile phone, normal forces larger that 1.2 N can result in excessive wear on the mating surfaces of these parts, which are often used to transmit electrical current [41].

The optimization problem statement used for substudies I–IV is

$$\min_{\phi_1} J = F \tag{7}$$

subject to

$$P < 0.15 \tag{8}$$

$$0 < F \leq 1.2 \text{ N} \tag{9}$$

and

$$0 \leq \phi_1 \leq 90 \text{ deg} \tag{10}$$

where F is the reaction force at the point of the applied deflection and P is the fraction of nodes that have plastically deformed.

During the optimization procedure, only the material orientation $\phi_{1,i}$ is changed, where i represents the ith homogeneous material segment, such as a single layer. For isotropic and single anisotropic layer L-beams, $i \in \{1\}$. For the laminated L-beam four layers are considered, so $i \in \{1,2,3,4\}$. Also, the heterogeneous L-beam is divided into two segments; therefore, $i \in \{1,2\}$. The material used throughout the case study is pure copper, which for substudies II–VI has been rolled and heat treated to create a very strong texture in the rolling direction. As a note, all material microstructures were obtained by measuring the microstructure of the sample as described in Sec. 3.2. In consideration of manufacturing process simplicity, we only allow material orientations belonging to the set {0 5 10 15 20 25 30 35 40 45 50 55 60 65 70 75 80 85 90} expressed in degrees.

Each of the substudies presented in this section used a genetic

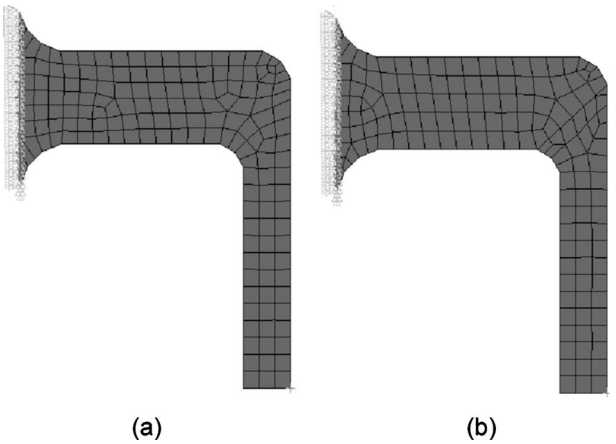

Fig. 7 (*a*) Finite element mesh for the isotropic, single layer, and four layer L-beams; (*b*) finite element mesh for the heterogeneous L-beam

algorithm to find the material orientation that minimized the reaction force, and ensured compliance with a material yielding criteria. The genetic algorithm was selected as the optimization algorithm as it is capable of searching over a design space with multiple local minima. Since we are interested in potentially orienting multiple layers, and since the orientation of each layer influences the effective properties of the part as a whole, many local minima exist in the design space. Due to the nature of genetic algorithms, it is possible for the optimization routine to converge on different solutions—which may or may not be the global optimal solution—for different optimization runs. To increase the likelihood that the global optimal solution is found, the optimization routine was executed multiple times for each substudy. For the examples presented in this paper, each run of the optimization routine resulted in approximately the same solution for a given substudy. The genetic algorithm parameters were the same for each of the substudies presented in this paper, which are as follows: a population size of 30 individuals, a maximum number of 30 generations, a mutation rate of 0.01, and a crossover rate of 0.50. While the optimization was permitted to run up to 30 generations, an optimal solution was often found within ten generations. As a note, these same algorithm parameters are used in substudies V and VI.

The genetic algorithm was coupled with the commercial finite element analysis software ANSYS to analyze the force and stresses of the structure. A material stiffness matrix—determined by the microstructure and the respective orientation—was input into ANSYS (using anisotropic element shell281), which then output the force required to achieve the prescribed deflection of the L-beam and also output a 6×1 stress vector for each node (refer to Fig. 5(*b*)). As a reference, the mesh used for substudies I–III, V, and VI may be seen in Fig. 7(*a*), and the mesh used for substudy IV may be seen in Fig. 7(*b*), where a line at approximately 45 deg separates the horizontal and vertical beams for the heterogeneous material. The 6×1 stress vector is then analyzed by the failure criteria presented in Sec. 2.4 to determine if failure has occurred. Using a Xeon 3.4 GHz processor and 3.25 Gbytes of RAM, the analysis took roughly 25 s per individual. This time includes both the genetic algorithm calculations and finite element analysis.

We now briefly provide additional information regarding each substudy and refer the reader to Tables 1 and 2 for the summary of the results.

4.1.1 Substudy I: Single Isotropic Layer L-Beam. The single layer isotropic L-beam is considered the benchmark design in this study as it is based on the same assumptions used in the design of the mobile phone previously mentioned. Namely, those assumptions are that the material used is isotropic, homogeneous, and linear elastic. With the material being isotropic, layer orientation has no effect on the performance, as shown in Table 1. As this is the benchmark design, all other substudies seek improved performance over the benchmark.

4.1.2 Substudy II: Single Anisotropic Layer L-Beam. Often, significant performance improvements can be achieved solely by capitalizing on the material anisotropy. We demonstrate this by showing performance increases that can be achieved in the same L-beam when created with a single anisotropic layer. This approach is beneficial as it only requires the material to be strategically oriented during the manufacturing process and does not require additional equipment such as an ultrasonic consolidation welder. By single layer orientation alone, as shown in Table 1, the performance increases are notable.

4.1.3 Substudy III: Multilayer Anisotropic L-Beam. By implementing ultrasonic consolidation (Sec. 2.1), the L-beam may be created with multiple thin layers, each independently oriented, to achieve a desired performance. While the multilayered material strategy may be more expensive to manufacture, it has a distinct advantage in that the design space significantly expands upon using a layered material approach. However, as shown in Table 1, the multilayered case cannot outperform the single layered case. Substudies V and VI explore this in further details, and illustrate that under different design objectives, the multilayered case will outperform the single layer case.

Table 1 Optimization results for the four material strategies presented in the L-beam case study. Angles are expressed in degrees.

Case	F (N)	P	$\phi_{1,1}$	$\phi_{1,2}$	$\phi_{1,3}$	$\phi_{1,4}$
(I) Benchmark	1.302	0.227	Isotropic	-	-	-
(II) Single layer	0.846	0.087	70	-	-	-
(III) Four layers	0.846	0.087	70	70	70	70
(IV) Heterogeneous	0.744	0.056	60	15	-	-

Table 2 Optimization results for the single and four layer L-beams with a target force and percent failure. Angles are expressed in degrees.

Case	F (N)	P	F_t (N)	P_t	$\phi_{1,1}$	$\phi_{1,2}$	$\phi_{1,3}$	$\phi_{1,4}$
(V) Single layer	0.99	0.101	0.98	0.12	0	-	-	-
(VI) Four layers	0.98	0.121	0.98	0.12	10	0	5	15

4.1.4 Substudy IV: Single Layer Heterogeneously Anisotropic L-Beam. We now consider a single layer case where the anisotropy throughout that layer is heterogeneous. For this example, $i=1$ represents the segment of the L-beam that is in aligned with the y-axis, and $i=2$ represents the segment that is aligned with the z-axis, as seen in Fig. 6. Through the exploration afforded by the optimization procedure, these two segments may take on any layer orientation, independent of the other. Using this approach, the improvement over the benchmark design is even more significant, as shown in Table 1.

In consideration of the manufacturing process that might be used to create such a heterogeneous microstructure, we propose a friction stir welding (FSW) process [40]. While various metal joining processes could be used to join the separate materials, FSW is desirable because it is a low temperature metal joining process. Since the material microstructure is designed to enable a specific performance, it is important that manufacturing processes do not significantly modify the material microstructure. The high temperature of traditional welding significantly changes the material microstructure at the weld site.

4.1.5 Results and Comparison for Substudies I–IV. Now we compare the numerical results of the four substudies presented in this case study, which are summarized in Table 1. Notice the values of the benchmark design with the isotropic material. Recalling that the maximum allowable force for this L-beam is 1.2 N, the benchmark design fails by exceeding the maximum allowable force and also by plastically deforming since P is greater than the allowable 0.15 or 15%. Simply by using a single anisotropic layer strategically oriented, we are able to meet the design objectives. Notice that the single layer and multilayered anisotropic material provide identical solutions. The reason for this is that the design objective seeks an extreme solution (i.e., minimize reaction force). Because it is an extreme solution, and not one in the center of the design space—which is the space that can be obtained by a multilayered laminate—the single layer laminate can provide an optimal solution. A more in-depth discussion of this is provided in Sec. 4.2. As a final note, we can see that further improvement on the design can be achieved when a heterogeneous material strategy is taken.

4.2 Substudies V and VI. Having observed in Sec. 4.1 that the multilayered anisotropic approach did not outperform the single layer anisotropic approach, we now consider the conditions under which it would. Before describing the new conditions, it is important to note that aside from the new optimization problem statement described below, all other conditions are identical to those of substudies I–IV. This includes all genetic algorithm parameters, and finite element parameters and meshes.

4.2.1 Substudy V: Multilayer L-Beam with Targets F and P. Recall the discussion on the range of material properties that can be achieved by rotation and lamination, and Fig. 4 in Sec. 2.5. It is difficult, if not impossible, to obtain even a few of the material properties enclosed by the property closure without utilizing a multilayered material approach. Substudy V illustrates this point. The following optimization problem statement searches for a design that provides a specific reaction force F_t and a specific fraction of yielding P_t by orienting four layers

$$\min_{\phi_1} J = (F - F_t)^2 + (P - P_t)^2 \tag{11}$$

subject to

$$P < 0.15 \tag{12}$$

$$0 < F \leq 1.2 \text{ N} \tag{13}$$

and

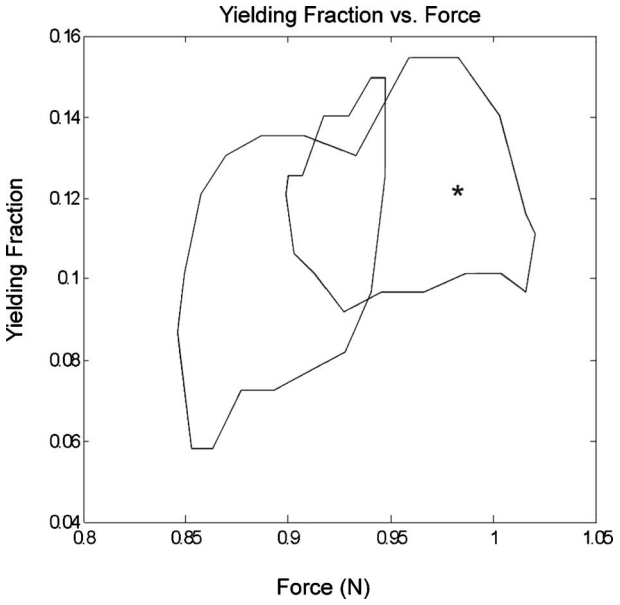

Fig. 8 Graphical representation of the feasible design space obtainable with rotations and laminations of the copper material used for substudies V and VI

$$0 \leq \phi_1 \leq 90 \text{ deg} \tag{14}$$

As a reference, $i=1$ represents the top layer of the L-beam and $i=4$ represents the bottom layer. The target force and node yielding fraction are 0.98 N and 0.12, respectively. As shown in Table 2, the multilayered case is capable of reaching the target performance. This is in contrast to the single layer case, which is described now.

4.2.2 Substudy VI: Single Layer L-Beam with Targets F and P. Here we revisit substudy V, with the modification that only one layer is possible—in contrast to the four layers considered in substudy V. It is interesting to note that by using a single layer, only a force of 0.99 N can be achieved with a plastic yielding fraction of 0.101. Figure 8 provides a graphical look at the nature of substudies V and VI. The horizontal axes represents the reaction force F, and the vertical axes represents the yielding fraction P of the part. The solid path represents the performance combinations that are possible using only a single layer. The path and the *area enclosed by the path* can be achieved by the multilayered lamination. To illustrate more fully, we choose a point within the path and set the corresponding values of F and P to F_t and P_t. This point is represented by the star in Fig. 8. The best values that can be afforded by the single layer approach is shown in Table 2.

We now return to the notion of making the hardware more difficult to reverse engineer. Consider for a moment using this L-beam as a mechanical fuse. One that explicitly requires a plastic yielding fraction of 0.12 at a reaction force of 0.98 N. Because this design point is *within* the area created by the solid lines in Fig. 8, a competitor can only find this design through a multilayered approach. Any design found by a single layer would be limited to the solid path in Fig. 8. While the single layer may be easier to manufacture, it comes at the expense of achieving the desired force and percent failure values.

Using the developments presented in Ref. [42], it can be shown that the barrier to reverse engineering for all the substudies is significantly larger than the barrier to reverse engineer the benchmark design. This can be explained by the additional exploration required to determine the layer orientation, or heterogeneity associated with the nonbenchmark designs.

In summary, we note that the following barriers exist for a competitor reverse engineering the hardware: (i) discovering that

a layering approach was used would be difficult and would require sophisticated microscopy; (ii) deciphering the microstructure created by the layering approach would be difficult even for those experienced with microstructure analysis; and (iii) determining the methodology to manufacture the microstructure, if it was deciphered, would be yet another challenge—perhaps one that is prohibitive.

5 Concluding Remarks

We have presented an approach that uses material microstructure information, numerical optimization, and state-of-the-art manufacturing techniques to create designs with a customized mechanical performance that is difficult to reverse engineer—a powerful combination for companies who wish to make innovative products and devices available to the masses without disclosing the phenomena that gives the device its customized performance. The root of the method is in manipulating the material microstructure numerically, while constrained to existing manufacturing methods (rolling, UC, and FSW). The consideration of these manufacturing approaches is embodied in the rotation/lamination theory and in the minimal negative effect that these joining processes have on the microstructures of interest. A simple study of a L-beam was presented to illustrate the basic benefits that come from the presented design and optimization approach. The case study considered one layer isotropic lamina, one layer anisotropic lamina, multilayered anisotropic laminae, heterogeneously distributed microstructures in single layer lamina, and a special exploration into when multilayered laminae outperform single layer lamina and vice-versa. Through this case study we see that by using a microstructure sensitive design approach, coupled with numerical optimization, product performance can be customized, and can be made manufacturable and difficult to reverse engineer. Difficult to reverse engineer because each scenario in the case study has identical geometry and material alloy, yet notably different performances, which can only be traced to difficult-to-discern microstructures. Ongoing research by the authors includes the exploration of additional microstructure manipulation strategies, quantification of barriers to reverse engineering as affected by the microstructure manipulation strategy, and a life cycle and return on investment analysis that is used to characterize the cost of such a design approach.

Acknowledgment

This research was partially supported by National Science Foundation (Grant No. CMMI-0800904) for C.A.M. and B.L.A.

Nomenclature

$\alpha_{ij}^{(s)}$ = combination of slip directions and slip plane normal for the sth slip system

C_{11} = material property constant obtained from the literature for selected material class

C_{12} = material property constant obtained from the literature for selected material class

C_{44} = material property constant obtained from the literature for selected material class

$\bar{C}_{wxyz}$ = sample stiffness (average crystal stiffness)

D^* = critical strain rate

$\bar{D}$ = macroscopic strain rate

D_k^N = normal direction of the kth lamina, also an axis for the lamina reference frame

D_k^R = rolling direction of the kth lamina, also an axis for the lamina reference frame

D_k^T = transverse direction of the kth lamina, also an axis for the lamina reference frame

δ = prescribed displacement

F = force

F_m = Fourier coefficients representing volume fraction of crystals in the mth bin of the fundamental zone

g = Euler angles from sample to crystal reference frames

g_{wx} = orientation matrix of Euler angles from sample to crystal reference frames

$\dot{\gamma}_0$ = reference shear rate

J = aggregate optimization objective statement

M = material class (e.g., nickel, copper)

M_0 = selected alloy from material class

μ = design objective

N = number of laminae to be used in layer-by-layer creation of material

n_c = number of columns in the binned fundamental zone

n_h = number of layers in the binned fundamental zone

n_r = number of rows in the binned fundamental zone

ν = constraint violation

$\phi_{1,n}$ = lamination orientation for the nth layer

S = slip systems, comprised of slip plane normals $\{111\}$ and slip directions $\langle 110 \rangle$

σ_i = 6×1 stress vector for the ith node

σ'_{kl} = deviatoric stress

τ = shear stress

$\tau^{*(s)}$ = critical resolved shear stress for the sth slip system

Subscripts and Superscripts

$[\,]_p$ = part reference frame

$[\,]_c$ = crystal reference frame

$[\,]_l$ = lamina reference frame

$[\,]^*$ = effective property unless otherwise noted

$[\,]_t$ = target value

References

[1] Afshar, M. H., 2008, "Layout and Size Optimization of Tree-Like Pipe Networks by Incremental Solution Building Ants," Can. J. Civ. Eng., **35**, pp. 129–139.

[2] Lassila, T., 2009, "Optimal Damping of a Membrane and Topological Shape Optimization," Struct. Multidiscip. Optim., **38**, pp. 43–52.

[3] Kumar, A. V., and Gossard, D. C., 1996, "Synthesis of Optimal Shape and Topology of Structures," ASME J. Mech. Des., **118**, pp. 68–74.

[4] Tavakoli, R., and Davami, P., 2009, "Optimal Riser Design in Sand Casting Process With Evolutionary Topology Optimization," Struct. Multidiscip. Optim., **38**, pp. 205–214.

[5] Nelson, S. A., Parkinson, M. B., and Papalambros, P. Y., 2001, "Multicriteria Optimization in Product Platform Design," ASME J. Mech. Des., **123**, pp. 199–204.

[6] Hariharan, K., and Balaji, C., 2009, "Material Optimization: A Case Study Using Sheet Metal-Forming Analysis," J. Mater. Process. Technol., **209**(1), pp. 324–331.

[7] Reed, R., and DeFillippi, R. J., 1990, "Casual Ambiguity, Barriers to Imitation, and Sustainable Competitive Advantage," Acad. Manage. Rev., **15**, pp. 88–102.

[8] McDowell, D. L., Choi, H.-J., Panchal, J., Austin, R., Allen, J., and Mistree, F., 2007, "Plasticity-Related Microstructure-Property Relations for Materials Design," Key Eng. Mater., **340–341**, pp. 21–30.

[9] Olson, G. B., 1997, "Computational Design of Hierarchically Structured Materials," Science, **277**, pp. 1237–1242.

[10] Kuehmann, C. J., and Olson, G. B., 2009, "Computational Materials Design and Engineering," Mater. Sci. Technol., **25**, pp. 472–478.

[11] Xia, Q., and Wang, M. Y., 2008, "Simultaneous Optimization of the Material Properties and the Topology of Functionally Graded Structures," Comput.-Aided Des., **40**, pp. 660–675.

[12] Chen, B. S., and Tong, L. Y., 2005, "Thermomechanically Coupled Sensitivity Analysis and Design Optimization of Functionally Graded Materials," Comput. Methods Appl. Mech. Eng., **194**, pp. 1891–1911.

[13] Adams, B. L., Nylander, C., Aydelotte, B., Ahmadi, S., Landon, C., Stucker, B. E., and Janaki-Ram, G. D., 2008, "Accessing the Elastic-Plastic Properties Closure by Rotation and Lamination," Acta Mater., **56**, pp. 128–139.

[14] White, D., 2003, "Ultrasonic Consolidation of Aluminum Tooling," Advanced Materials and Processes, **161**, pp. 64–65.

[15] Messac, A., and Mattson, C. A., 2004, "Normal Constraint Method With Guarantee of Even Representation of Complete Pareto Frontier," AIAA J., **42**(10), pp. 2101–2111.
[16] Mattson, C. A., and Messac, A., 2005, "Pareto Frontier Based Concept Selection Under Uncertainty, With Visualization," Optimization and Engineering, **6**(1), pp. 85–115.
[17] Mattson, C. A., Mullur, A. A., and Messac, A., 2004, "Smart Pareto Filter: Obtaining a Minimal Representation of Multiobjective Design Space, Engineering Optimization," Eng. Optimiz., **36**(6), pp. 721–740.
[18] Norton, R. L., 2006, *Machine Design*, Prentice-Hall, Upper Saddle River, NJ.
[19] Adams, B. L., Kalidindi, S. R., and Fullwood, D. T., 2005, *Microstructure Sensitive Design for Performance Optimization*, BYU Academic Publishing, Provo, UT.
[20] Hyer, M. W., 1998, *Stress Analysis of Fiber-Reinforced Composite Materials*, McGraw-Hill, New York.
[21] Mejia-Rodriguez, G., Renaud, J. E., and Tomar, V., 2008, "A Variable Fidelity Model Management Framework for Designing Multiphase Materials," ASME J. Mech. Des., **130**, p. 091702.
[22] Kolpakov, A. G., and Kolpakova, I. G., 1995, "Design of Laminated Composites Possessing Specified Homogenized Characteristics," Comput. Struct., **57**, pp. 599–604.
[23] McMahon, M. T., Watson, L. T., Soremekun, G. A., Gtirdal, Z., and Haftka, R. T., 1998, "A FORTRAN 90 Genetic Algorithm Module for Composite Laminate Structure Design," Eng. Comput., **14**, pp. 260–273.
[24] Sinke, J., 2006, "Development of Fibre Metal Laminates: Concurrent Multi-Scale Modeling and Testing," J. Mater. Sci., **41**, pp. 6777–6788.
[25] McDowell, D. L., 2000, "Modeling and Experiments in Plasticity," Int. J. Solids Struct., **37**, pp. 293–309.
[26] McDowell, D. L., 2001, "Materials Design: A Useful Research Focus for Inelastic Behavior of Structural Metals," Theor. Appl. Fract. Mech., **37**, pp. 245–259.
[27] Adams, B. L., Gao, X. C., and Kalidindi, S. R., 2005, "Finite Approximations to the Second-Order Properties Closure in Single Phase Polycrystals," Acta Mater., **53**, pp. 3563–3577.
[28] Daniels, H., 1965, "Ultrasonic Welding," Ultrasonics, **3**, pp. 190–196.
[29] O'Brien, R., 1991, *Welding Handbook*, American Welding Society, Miami, FL.
[30] Ram, G., Yang, Y., George, J., Robinson, C., and Stucker, B., 2006, "Improving Linear Weld Density in Ultrasonically Consolidated Parts," Proceedings of the 17th Solid Freeform Fabrication Symposium.
[31] Ram, G. D. J., Yang, Y., and Stucker, B. E., 2006, "Effect of Process Parameters on Bond Formation During Ultrasonic Consolidation of Aluminum Alloy 3003," J. Manuf. Syst., **25**, pp. 221–239.
[32] Ram, G. J., Robinson, C., Yang, Y., and Stucker, B., 2007, "Use of Ultrasonic Consolidation for Fabrication of Multi-Material Structures," Rapid Prototyping J., **13**, pp. 226–235.
[33] Bhattacharjee, P., Ray, R., and Upadhyaya, A., 2005, "Development of Cube Texture in Pure Ni, Ni–W and Ni–Mo Alloys Prepared by the Powder Metallurgy Route," Scr. Mater., **53**, pp. 1477–1481.
[34] Bunge, H., 1993, *Texture Analysis in Materials Science*, Cuvillier Verlag Gottingen, Gottingen, Germany.
[35] Hertzberg, R. W., 1989, *Deformation and Fracture Mechanics of Engineering Materials*, Wiley, New York.
[36] Fromm, B., Adams, B., Ahmadi, S., and Knezevic, M., 2008, "Grain Size and Orientation Distribution Function of High Purity Alpha-Titanium," Proceedings of the 15th International Conference on the Textures of Materials (ICOTOM15).
[37] Bata, V., and Pereloma, E., 2004, "An Alternative Physical Explanation of the Hall–Petch Relation," Acta Mater., **52**, pp. 657–665.
[38] Taylor, G. I., 1938, "Plastic Strain in Metals," J. Inst. Met., **62**, pp. 307–324.
[39] Asaro, R., and Needleman, A., 1985, "Texture Development and Strain Hardening in Rate Independent Polycrystals," Acta Metall. Mater., **33**, pp. 923–953.
[40] Owen, C. B., 2006, "Two Dimensional Friction Stir Welding Model With Experimental Validation," MS thesis, Brigham Young University, Provo, UT.
[41] Weight, B. L., Mattson, C. A., Magleby, S. P., and Howell, L. L., 2007, "Configuration Selection, Modeling, and Preliminary Testing in Support of Constant Force Electrical Connectors," ASME J. Electron. Packag., **129**, pp. 236–246.
[42] Harston, S. P., and Mattson, C. A., 2009, "Metrics for Evaluating and Optimizing the Barrier and Time to Reverse Engineer a Product," ASME Paper No. IDETC/CIE 2009, pp. C2009–C86781.